17th World Conference on Earthquake Engineering, 17WCEE
Sendai, Japan - September 13th to 18th 2020

SECOND-ORDER TWO-FIELD MIXED FORMULATION FOR SEISMIC ANALYSIS OF SHEAR-CRITICAL RC COLUMNS

A. Ayoub[(1)], D. Das[(2)]

[(1)] *Professor, City, University of London, ashraf.ayoub.1@city.ac.uk*
[(2)] *Ph.D. Candidate, City, University of London, dipankar.das.1@city.ac.uk*

Abstract

This study presents a new frame element formulation following a two-field Hellinger-Reissner functional for seismic analysis of shear-critical reinforced concrete (RC) members considering distributed inelasticity approach and large displacements effects. In the past, several types of frame elements have been developed, e.g. displacement-based and force-based models for analysis of RC columns. The two-field mixed-based fiber element formulation has been developed before for flexure-critical members, showing advantages over other existing elements. To simulate the shear-dominated failure modes, appropriate choice of beam theory along with multi-axial constitutive material models are needed to implement into the frame element formulation. Moreover, two-field mixed-based formulations also need the proper choice of both displacement and force shape functions which should satisfy both adopted section kinematics and stability criteria. Section kinematics equations have been derived considering Timoshenko beam theory. Stability criteria ensure that the adopted shape functions are suitable to render accurate response without needing any subsidiary conditions for the interpolation functions. In this research work, multi-axial stress interaction due to crack induced anisotropy has been adopted in the 2D reinforced concrete fiber by implementing the fixed smeared crack softened membrane model. Additionally, the effect of P-delta has been accounted for by adopting Green-Lagrange strain measures. The newly developed mixed-based frame element has been validated by examining various global and local response variables of experimentally tested RC columns under seismic loading conditions.

Keywords: mixed formulation; shear deformation; reinforced concrete; soften membrane model; seismic analysis; second order

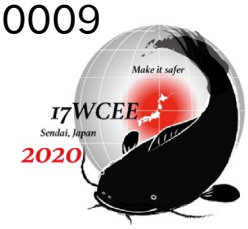

1. Introduction

Variational functionals and section level kinematics are in general needed to formulate conventional frame elements. For example, displacement-based formulation is based on potential energy functional whereas complementary energy functional is used for force-based formulation. On the other hand, for two-field mixed-based formulation, Hellinger-Reissner (HR) functional needs to be used. Also, we can use different types of section level kinematics such as Euler-Bernoulli and Timoshenko beam theories to simulate the experimentally observed behavior of flexure and shear critical members respectively. The principle argument for displacement-based and force-based formulation are nodal displacements and forces respectively. However, for two-field HR formulation, both nodal displacements and forces are the principle arguments. Therefore, displacement and force shape functions are coupled and special care needs to be considered to choose these shape functions to satisfy the required stability criteria.

2. Background

In the following, we will present frame element formulations based on distributed inelasticity approach considering both geometric linear and nonlinear cases.

The authors in [1] developed an equilibrium-based fiber frame element formulation considering parabolic distribution of shear strain following the micro-plane model for concrete proposed by [2] to include axial-flexure-shear interaction. A study in [3] presents a force-based fiber beam element formulation considering Timoshenko based section kinematics along with ad hoc nonlinear shear force-shear deformation law at the section level to include the shear effect. The study in [4] provided a literature review of fiber-based frame element formulations through various multi-axial material constitutive laws such as strut and tie models, micro-plane model, smeared crack models, damage models, etc. to simulate axial-flexure-shear interaction. All the frame elements formulated up to this time were based on either displacement based or force based.

So far, we have discussed about the frame element formulations based on undeformed configuration. In the following, we will present the research works considering nonlinear geometry effect. The authors in [5] developed a displacement-based corotational beam element using vectorial rotational variables along with uncoupled flexure-shear interaction. A study in [6] recently developed two fiber beam element formulations considering potential energy and HR functional for reinforced concrete components adopting only the axial-flexure interaction. Also, [7] proposed a three-field mixed-based (Hu-Washizu variational principle) corotational fiber beam element formulation following small deformation theory at the basic element level (without rigid body modes) considering damage-plastic concrete material law.

It can be noted that two types of fiber frame elements have been developed so far to consider both shear and nonlinear geometry effects i.e. displacement-based and three-field mixed-based. Other types of element formulations can be more robust, efficient and computationally less demanding i.e. two-field mixed and hybrid-based formulations. The newly developed two-field mixed-based formulation [8] has been extended to account for geometric nonlinearity effect for reinforced concrete members in the current research work.

3. Second-order mixed shear element

In this research work, a new shear-critical frame element based on distributed inelasticity approach, is developed following the HR variational principle, and considering geometric nonlinearity effect. The axis of the proposed frame element is a straight line joined by nodes I and J in the statically determinate basic reference system in which rigid body displacements are removed by choosing the simple supported boundary conditions as shown in Fig. 1. The frame element is composed of several sections along its axis.

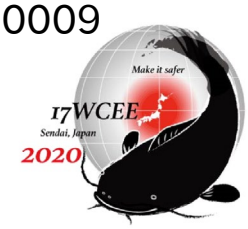

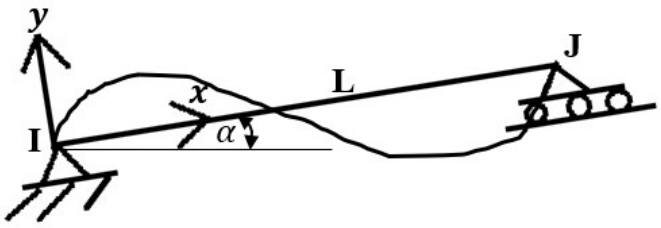

Fig. 1 – Basic reference system without rigid body modes

The element nodal displacement vector $\boldsymbol{u_{IJ}}$ collects the nodal displacement with respect to global axes. In the proposed frame element, an additional middle nodal rotational degree of freedom is included to satisfy stability criteria, which has been statically condensed out at the element level before the assembling process. The element deformation vector $\boldsymbol{v}$ collects the relative translation u at node J in X direction, rotations θ_z at nodes I and J and middle node k with respect to basic reference axes as shown in the Fig. 2.

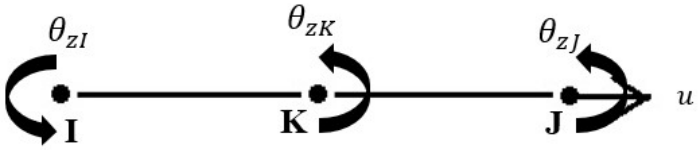

Fig. 2 – Element nodal deformations

The relation between element nodal deformation $\boldsymbol{v}$ and displacements $\boldsymbol{u_{IJ}}$ can be uniquely determined by the compatibility matrix $\boldsymbol{a_c}$ under deformed geometry conditions, where L is the deformed length of the element.

$$\boldsymbol{v} = \boldsymbol{a_c}\boldsymbol{u_{IJ}} \tag{1}$$

Where

$$\boldsymbol{a_c} = \begin{bmatrix} -\frac{1}{L}\sin\alpha & \frac{1}{L}\cos\alpha & 1 & \frac{1}{L}\sin\alpha & -\frac{1}{L}\cos\alpha & 0 & 0 \\ -\cos\alpha & -\sin\alpha & 0 & \cos\alpha & \sin\alpha & 0 & 0 \\ -\frac{1}{L}\sin\alpha & \frac{1}{L}\cos\alpha & 0 & \frac{1}{L}\sin\alpha & -\frac{1}{L}\cos\alpha & 1 & 0 \\ -\frac{1}{L}\sin\alpha & \frac{1}{L}\cos\alpha & 0 & \frac{1}{L}\sin\alpha & -\frac{1}{L}\cos\alpha & 0 & 1 \end{bmatrix} \tag{2}$$

Where,

$$L = \sqrt{((x_2 - x_1) + (u_J - u_I))^2 + ((y_2 - y_1) + (v_J - v_I))^2} \tag{3}$$

$$\sin\alpha = \frac{(y_2 - y_1) + (v_J - v_I)}{L} \tag{4}$$

$$\cos\alpha = \frac{(x_2 - x_1) + (u_J - u_I)}{L} \tag{5}$$

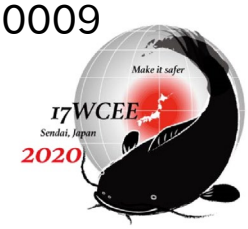

(x_1, y_1) *and* (x_2, y_2) are initial coordinates of nodes I and J respectively.

By introducing the section deformation vector $\boldsymbol{d}(x)$ which is a function of section displacement vector and material strain displacement vector $\boldsymbol{\varepsilon}(x, y)$, we can write down the below equation following the degenerated form of Green-Lagrange strain measures with the help of the section compatibility matrix $\boldsymbol{a}_s(y)$:

$$\boldsymbol{\varepsilon}(x, y) = \boldsymbol{a}_s(y)\boldsymbol{d}(x) \tag{6}$$

Where

$$\boldsymbol{d}(x) = \left[\frac{\partial u(x)}{\partial x} + \frac{1}{2}\left(\frac{\partial v(x)}{\partial x}\right)^2 \quad \frac{\partial \theta_z(x)}{\partial x} \quad \left(-\theta_z(x) + \frac{\partial v(x)}{\partial x}\right)\right]^T \tag{7}$$

$$\boldsymbol{d}(x) = \left[\varepsilon_0 \emptyset_z \gamma_y\right]^T \tag{8}$$

$$\boldsymbol{a}_s(y) = \begin{bmatrix} 1 & -y & 0 \\ 0 & 0 & 1 \end{bmatrix} \tag{9}$$

Where the axial strain ε_0 at the reference x axis, the curvature $\emptyset_z$ about the z axis and shear deformation γ_y in the y direction respectively.

The differential equilibrium equation of a segment of length dx of a reinforced concrete element, can be written down as follows:

$$\frac{dN_x}{dx} = 0 \tag{10}$$

$$\frac{dM_x}{dx} - V_x = 0 \tag{11}$$

$$\frac{dV_x}{dx} - \frac{d}{dx}\left(N_x \frac{dv(x)}{dx}\right) = 0 \tag{12}$$

where N_x, M_x, V_x are the axial force, bending moment and shear force respectively.

The section constitutive law is as follows:

$$\boldsymbol{D}(x) = f_{sec}(\boldsymbol{d}(x)) \tag{13}$$

Here f_{sec} is a non-linear function that relates the section force and deformation fields. The section is discretized with 2D fibres. Fibre integration is used to determine the section force-deformation relation. To couple normal and shear stresses at the material fibre level, multi-axial constitutive laws for materials are essential, which in turn help comprise the interaction of axial force, bending moment and shear force at the element section level. In this research work, the softened membrane model has been implemented [9] to simulate the biaxial interaction between normal and shear stress at the material fibre level.

HR energy functional can be written without body forces and surface tractions with section level variables in the following form:

$$\prod_{HR}(\boldsymbol{u}, \boldsymbol{p}) = -\int_0^L \boldsymbol{D}^T \boldsymbol{d}(\boldsymbol{D})\, dx + \int_0^L \widehat{\boldsymbol{D}}^T(\boldsymbol{p})\boldsymbol{d}(\boldsymbol{u})\, dx - \boldsymbol{u}^T \boldsymbol{P}^* \tag{14}$$

In this element formulation, the beam section forces $\widehat{\boldsymbol{D}}$ are independently derived from the element nodal forces $\boldsymbol{p}$ degree of freedom as follows:

$$\widehat{\boldsymbol{D}}(x) = \boldsymbol{b}(x)\,\boldsymbol{p} \tag{15}$$

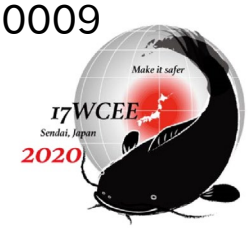

Here $\boldsymbol{b}(x)$ is the matrix of force interpolation function.

By taking variation of Equation (14) and linearizing the variation, and using Equations (8), (13), and (15) along with the assumption of conservative external load and from arbitrariness of $\delta\boldsymbol{u}$ and $\delta\boldsymbol{p}$, the following equation can be written at equilibrium:

$$\begin{bmatrix} \int_L \frac{\partial}{\partial \boldsymbol{u}}(\boldsymbol{B}_s^T\boldsymbol{b}(x))\boldsymbol{p}dx & \int_0^L \boldsymbol{B}_s^T\boldsymbol{b}dx \\ \int_0^L \boldsymbol{b}^T\boldsymbol{B}_s\,dx & -\int_0^L \boldsymbol{b}^T\boldsymbol{f}_s\boldsymbol{b}dx \end{bmatrix}\begin{pmatrix}\Delta\boldsymbol{u}\\ \Delta\boldsymbol{p}\end{pmatrix} = \begin{pmatrix}\boldsymbol{P}^* - \int_0^L \boldsymbol{B}_s^T\boldsymbol{D}dx \\ \int_0^L \boldsymbol{b}^T(\widehat{\boldsymbol{d}} - \boldsymbol{d})dx\end{pmatrix} \tag{16}$$

where $\boldsymbol{f_s}(x)$ is the section flexibility matrix, $\boldsymbol{B_s}(x)$ is the strain displacement matrix which is a function of $\boldsymbol{u}(x)$, and $\widehat{\boldsymbol{d}}(x)$ is the section deformation vector determined from section force vector $\widehat{\boldsymbol{D}}(x)$ with the help of the section flexibility matrix.

Equation (16) can be written in the following concise form:

$$\begin{bmatrix}\boldsymbol{K}_{ig} & \boldsymbol{G}^T \\ \boldsymbol{G} & -\boldsymbol{F}_{c+s}\end{bmatrix}\begin{pmatrix}\Delta\boldsymbol{u}\\ \Delta\boldsymbol{p}\end{pmatrix} = \begin{pmatrix}\boldsymbol{P}^* - \boldsymbol{P}_{c+s}^r \\ \boldsymbol{u}^r\end{pmatrix} \tag{17}$$

Here, $\boldsymbol{F}_{c+s}$ is the element flexibility matrix, $\boldsymbol{G} = \int_0^L \boldsymbol{b}^T\boldsymbol{B}_s\,dx$, $\boldsymbol{u}^r$ is the element residual deformation vector, and $\boldsymbol{K}_{ig}$ is the internal geometric stiffness matrix.

After the static condensation of the force fields at the element level, Equation (17) becomes:

$$\left[\boldsymbol{K}_{ig} + \boldsymbol{G}^T[\boldsymbol{F}_{c+s}^{-1}]\boldsymbol{G}\right]\Delta\boldsymbol{u} + \boldsymbol{G}^T[\boldsymbol{F}_{c+s}^{-1}][-\boldsymbol{u}^r] = \boldsymbol{P}^* - \boldsymbol{G}^T\boldsymbol{P}_{c+s}^r \tag{18}$$

Once convergence is reached at the element level, i.e. $\boldsymbol{u}^r$ becomes zero, Equation (18) can be written as follow:

$$(\boldsymbol{K}_{ig} + \boldsymbol{G}^T[\boldsymbol{F}_{c+s}^{-1}]\boldsymbol{G})\Delta\boldsymbol{u} = \boldsymbol{P}^* - \boldsymbol{G}^T\boldsymbol{P}_{c+s}^r \tag{19}$$

Details of the internal geometric stiffness matrix $\boldsymbol{K}_{ig}$, the external geometric stiffness matrix $\boldsymbol{K}_{og}$ and state determination process can be found in [9].

4. Correlation studies

This section presents several correlation studies of the newly developed element with the experimental results of reinforced concrete and composite members for cyclic loading condition for both geometric linear and nonlinear scenarios to demonstrate the capability of the element formulation to simulate accurately global and local response with implemented multi-axial material model.

4.1 Column by Imai and Yamamoto [10]

The authors in [10] conducted cyclic tests of reinforced concrete columns under constant axial compressive loading of 392 kN with increasing amplitude of lateral displacement cycles at the columns top end. The specimen has width and depth of 400 mm and 500 mm respectively. 14 longitudinal reinforcements of diameter 22 mm are uniformly spaced along the perimeter of the columns. Rectangular hoops of diameter 9 mm are placed at a spacing of 100 mm along the length of the columns. The concrete compressive strength of the column is 27.1 MPa. Yield strengths of longitudinal and transverse reinforcements are 318 MPa and 336 MPa respectively. One element has been used to model the entire column specimen with 5 section integration points. Fig. 3 compares the lateral load versus top end deflection response of the models using the proposed beam element with the experimental results. It can be observed from the plot that the proposed element can capture the loading capacity and pinching effect of hysteretic behaviour reasonably well.

However, some divergence in results can be observed in the last loading cycle as the shear resisting mechanisms invoked during this loading stage has not been included in the element model.

It can be observed from Fig. 3 that we need to have mixed shear element which can reasonably reproduce experimentally observed load deformation response for shear critical members, while the mixed flexure element overestimates the shear capacity and stiffness both.

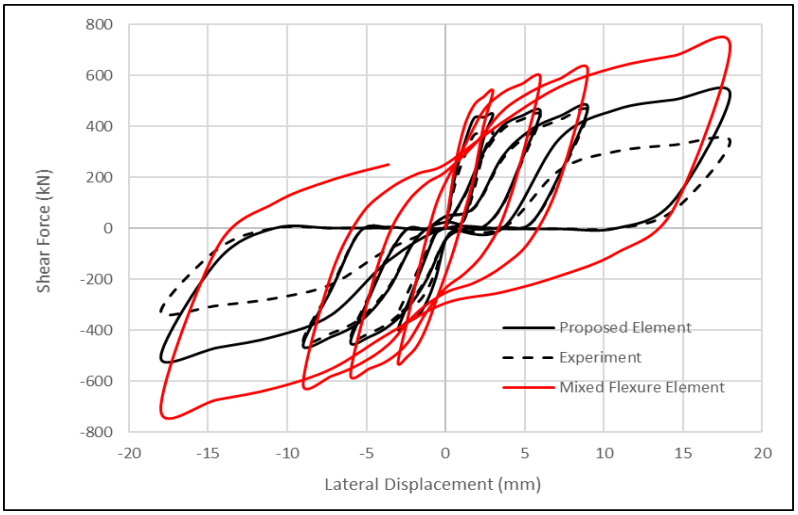

Fig. 3 – Lateral load-deflection response (geometric linear)

4.2 Column by Legeron and Paultre [11]

The authors in [11] performed tests on a series of 6 large-scale cantilever reinforced high strength concrete columns (shear span ratio=6.56) under constant axial compressive load and reverse cyclic lateral loading to investigate primarily the effect of axial load on seismic behaviour of slender columns. Out of these columns, Specimen 5 is chosen for the correlation study. The specimen has been subjected to a constant axial load of 2400 kN. The specimen has width and depth both of 305 mm and length of 2000 mm. 4 corner longitudinal reinforcements of diameter 19.5 mm and 4 intermediate longitudinal reinforcements of diameter 16 mm are uniformly spaced along the perimeter of the columns. Square hoops of diameter 11.3 mm are placed at a spacing of 130 mm along the length of the columns. The concrete compressive strength of the column is 97.7 MPa. Yield strengths of corner and middle longitudinal and transverse reinforcements are 430 MPa, 494 MPa and 391 MPa respectively. One element has been used to model the entire column specimen with 5 section integration points. Fig. 4 compares the lateral load versus top end deflection response of the models using the proposed beam element with the experimental result.

From the Fig. 4, it can be observed that the proposed element without P-Delta effects overestimates the shear strength and stiffness as expected. Whereas the proposed element with P-Delta effect has exceptionally reproduced the overall experimentally observed load-deflection response. Stiffness, shear resistance, shear deformation capacity along with hysteretic behaviour have been captured very well.

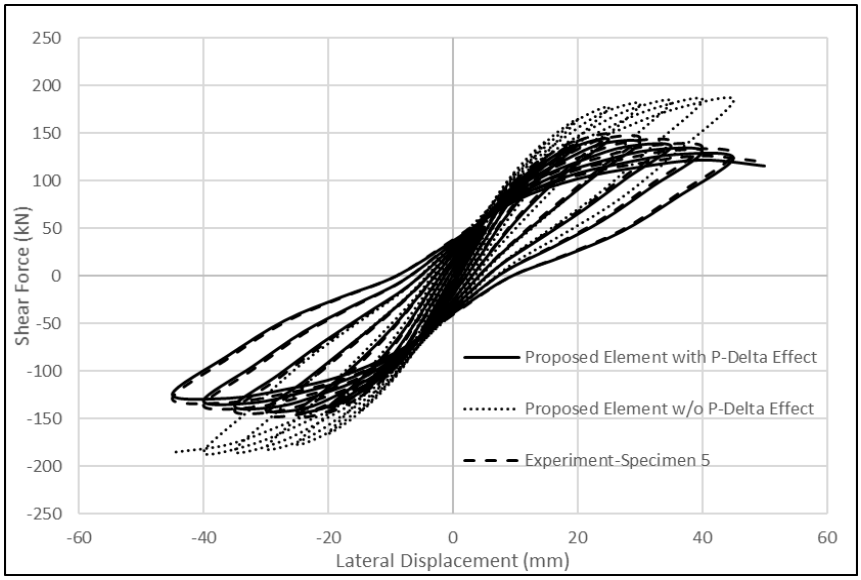

Fig. 4 – Load-deflection response of specimen 5

4.3 Wall by Epackachi et al. [12]

The authors in [12] conducted an experimental study to investigate the behaviour of large-scale steel-plate composite (SC) walls subjected to displacement-controlled cyclic lateral loading representative of seismic loading. The testing program involved four rectangular SC wall specimens with an aspect ratio (height-to-length) of 1.0. The studs and tie rods are spaced at distance 102 mm and 305 mm respectively, the height, length and overall thickness of the wall is 1524mm, 1524mm and 305 mm respectively, the thickness of each faceplate is 4.8mm, the reinforcement ratio is 3.1%, the faceplate slenderness ratio is 21, and concrete strength measured on the day of the tests is 31MPa. The diameters of the studs and tie rods were 9.5 mm for all walls. The studs and tie rods were fabricated from carbon steel with nominal yield strength of 345 MPa. The yield and ultimate strengths of the steel faceplates, calculated from three coupon tests, were 262 and 380 MPa, respectively. The SC1 wall is modelled and validated against experimental results as shown in Fig. 5 and 6. It can be seen that pinching of the load deformation response as observed in experimental testing is not captured in the analytical load deformation response (Normal Concrete (NC)-Blue Colour) as the present model does not include the plate buckling and bond-slip behaviour which are primary load resisting mechanism in case of economically designed SC wall along with flexural-shear failure of concrete. However, the present model can capture the peak shear strength, initial stiffness, deformation capacity, and energy dissipation with reasonable accuracy. Henceforth, the same model has been used to investigate the effect of fibre on load-deformation characteristics. The concrete compressive and tensile strength of an assumed steel fiber-volume ratio V_f= 1% are 40.85 MPa and 4.7 MPa respectively. The concrete compressive and tensile strength of an assumed carbon nano fibre V_f= 1% are 32.75 MPa and 4.48 MPa respectively. It can be seen that SFRC 1% and CNF 1% provide better overall performance than that of NC. In addition, 1% SFRC provides more initial stiffness and peak shear strength but less energy dissipation and deformation capacity than that of 1% CNF. The similar observation for SFRC has been reported by several researchers in case of reinforced concrete members.

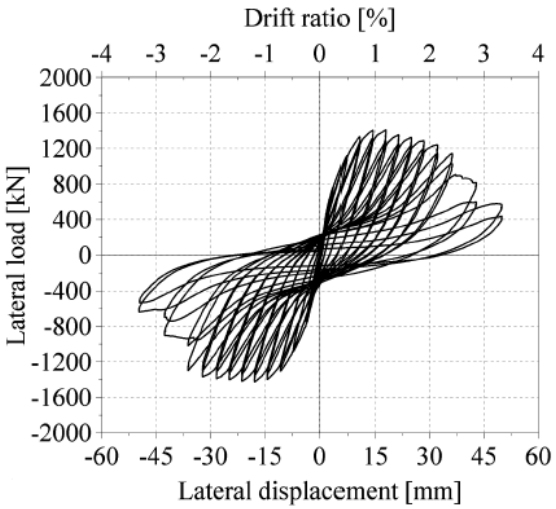

Fig. 5 – Experimental load-deflection of SC1

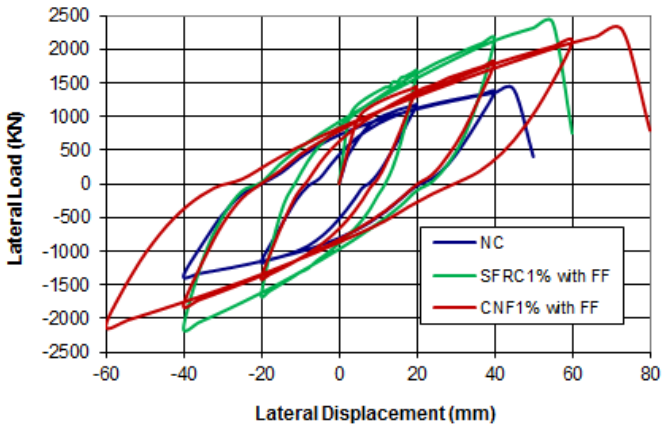

Fig. 6 – Numerical load-deflection curve

It has been seen from the experiment of flexure-shear critical SC1 specimen that double skin composite walls subjected to cyclic loading primarily failed from local buckling of the steel plates and subsequent concrete crushing and tie bar fracture. Due to the residual tensile strain, a large compressive stress developed early while steel face plates subjected to reverse cyclic loading. However, the steel plate became susceptible to buckling due to the filled unreinforced normal concrete could not resist compression under tensile strains. After buckling of the steel plates occurred, excessive compressive force was imposed on the filled unreinforced normal concrete. Moreover, the buckled steel plates could not provide lateral confinement to the filled unreinforced normal concrete. Thus, the crushing of the concrete and fracture of the tie bars followed the buckling of the steel plates. Thus, the development of accumulated plastic tensile strain in the plate can become a measure of progression of steel plate buckling. The present model does not consider the buckling of steel plate. However, the effect of fibre on buckling phenomenon can be indirectly captured by plotting the longitudinal steel strain of the most critical fibre i.e. the outermost fibre.

It can be observed from Fig. 7 that the progression of accumulated plastic strain in the plate is higher for normal concrete than that of 1% SFRC and 1% CNF while the latter has shown lesser rate of progression of accumulated plastic tensile strain. Thus, it can be concluded that CNF and SFRC are both effective in delaying the buckling phenomenon.

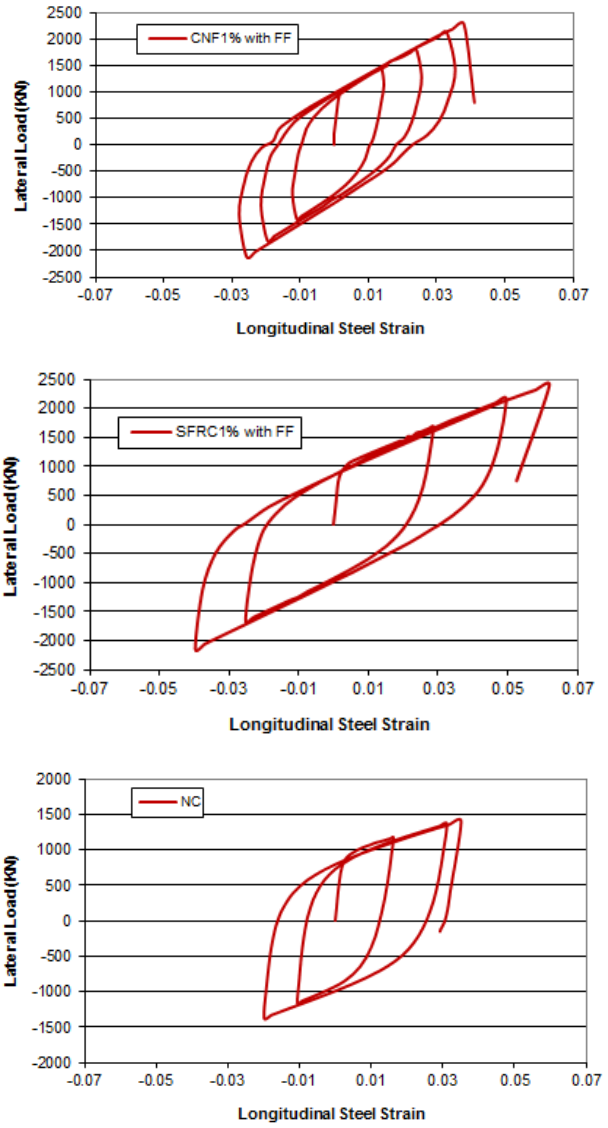

Fig. 7 – Longitudinal steel strain at outermost fibre

5. Conclusion

It can be concluded that the proposed mixed-based shear beam element including geometric nonlinearity effect, successfully reproduced global and local behaviour for the case of flexure and shear failure modes under both monotonic and cyclic loading conditions. The need of mixed-based shear element with large displacement effect to formulate inelastic analysis-driven design process has been established through this research work. A consistent variational framework of frame element formulations for determining element tangent stiffness and resistance matrix has been developed, which will be very useful in the development of performance-based design procedures for reinforced concrete structures.

6. References

[1] Petrangeli M, Pinto PE, Ciampi V (1999): Fibre element for cyclic bending and shear of RC structures. I: theory. *Journal of Engineering Mechanics*, 125 (9), 994-1001.

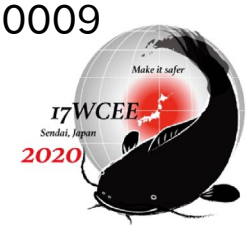

[2] Bazant ZP, Oh BH (1985): Microplane model for progressive fracture of concrete and rock. *Journal of Engineering Mechanics, ASCE,* 111(4), 559–582.

[3] Marini A, Spacone E (2006): Analysis of reinforced concrete elements including shear effects. *ACI Structural Journal,* 103(5), 645–655.

[4] Ceresa P, Petrini L, Rui P (2007): Flexure–shear fiber beam-column elements for modeling frame structures under seismic loading-state of the art. *J Earthq Eng*, 11(1), 46–88.

[5] Long X, Tan KH, Lee CK (2013): A 3D co-rotational beam element for steel and RC framed structures. *Struct Eng Mech*, 48(5), 587-613.

[6] Gendy SSFM, Ayoub A (2018): Displacement and mixed fibre beam elements for modelling of slender reinforced concrete structures under cyclic loads. *Engineering Structures*, 173, 620–630.

[7] Paolo DR, Addessi D (2018): A mixed 3D corotational beam with cross-section warping for the analysis of damaging structures under large displacements. *Meccanica*, 53, 1313–1332.

[8] Das D, Ayoub A (2019): Mixed formulation of inelastic composite shear beam element. *J. Struct. Eng.,* (Accepted).

[9] Das D (2019): Mixed formulation for seismic analysis of shear critical reinforced concrete, steel and composite structures. *Doctoral thesis*, City, University of London.

[10] Imai H, Yamamoto Y (1986): A study on causes of earthquake damage of Izumi high school due to Miyagi-Ken-Oki earthquake in 1978. *Trans Jpn Conc Inst*, 8, 405-418.

[11] Le´geron F, Paultre P (2000): Behavior of high-strength concrete columns under cyclic flexure and constant axial load. *ACI Struct J*, 97(4), 591–601.

[12] Epackachi S, Nam HN, Efe GK, Andrew SW, Amit HV (2014): In-plane seismic behavior of rectangular steel-plate composite wall piers. *American Society of Civil Engineers*, DOI:10.1061/(ASCE)ST, 1943-541, X.0001148.

